Robust lesion network mapping reveals genuine symptom-specific networks

Weigang Cui[1,†], Jiayi Zhu[1,2,†], Yang Long[1,2,†], Yilin Yin[1,3], Wei Zhang[1], Jianting Huang[1], Feng Wang[4], Evan M. Gordon[5,6], Nico U.F. Dosenbach[5,6,7,8,9,10], Danhong Wang[1], Jianxun Ren[1,*], Hesheng Liu[1,11,*]

[1] Changping Laboratory, Beijing, China

[2] State Key Laboratory of Cognitive Neuroscience and Learning, Beijing Normal University, Beijing, China

[3] Genetic Diseases Key Laboratory of Sichuan Province, Medical Genetics and Rare Diseases Center, Department of Laboratory Medicine, Sichuan Provincial People's Hospital, School of Medicine, University of Electronic Science and Technology of China, Chengdu, China

[4] Department of Neurosurgery, The First Affiliated Hospital of Fujian Medical University, Fuzhou, China

[5] Mallinckrodt Institute of Radiology, Washington University School of Medicine, St Louis, MO, USA

[6] Allied Labs for Imaging Guided Neurotherapies (ALIGN), Washington University School of Medicine, St Louis, MO, USA

[7] Department of Neurology, Washington University School of Medicine, St Louis, MO, USA

[8] Department of Biomedical Engineering, Washington University in St. Louis, St Louis, MO, USA

[9] Department of Psychological and Brain Sciences, Washington University in St. Louis, St Louis, MO, USA

[10] Department of Pediatrics, Washington University School of Medicine, St Louis, MO, USA

[11] Biomedical Pioneering Innovation Center, Peking University, Beijing, China

[†] These authors contributed equally: Weigang Cui, Jiayi Zhu, Yang Long.

[*] Address correspondence to: Dr. Hesheng Liu (hesheng@biopic.pku.edu.cn) or Dr. Jianxun Ren (Jianxun.ren@cpl.ac.cn)

Abstract

Lesion network mapping (LNM) and its derivatives successfully integrate anatomically distributed brain loci into common symptom-associated functional networks. However, their statistical validity and specificity have recently become topics of debate. Here, we introduce a null model-based robust LNM (rLNM) framework to perform sensitivity and symptom-specificity testing. Across multiple lesion-based (10 conditions, 333 lesions) and task-based (4 conditions, 706 experiments) datasets, rLNM reveals biologically meaningful and symptom-specific networks while effectively controlling for false positives.

Main Text

Lesion network mapping (LNM) aims to identify the neural substrates underlying specific neuropsychiatric symptoms by associating anatomically heterogeneous lesions with common functional networks[1]. This technique has been extended from focal lesions to task activations[2], atrophy patterns[3], and brain stimulation sites[4]. Despite its broad adoption, LNM has recently come under methodological scrutiny, with critiques suggesting that the network patterns reported across diverse disorders are highly similar, and may primarily reflect the hub architecture of the normative connectome rather than disorder-specific circuitry[5]. Subsequent studies have countered that this similarity is overstated[6-10], providing evidence that genuine symptom-specific functional networks do exist despite their entanglement with underlying connectome structure. However, conventional LNM still lacks a rigorous statistical framework to distinguish genuine network effects from connectome-driven biases.

In most implementations, conventional LNM consists sensitivity[9] and specificity[6] testing. Sensitivity testing identifies voxels at which lesion-connectivity overlap, the proportion of lesions showing significant functional connectivity, exceeds an arbitrarily-chosen threshold applied uniformly across the brain (e.g., ≥75%). However, hub regions inherently show higher overlap than non-hub regions, so this approach inflates false positives at hubs and false negatives elsewhere. Specificity testing is conventionally performed by contrasting the symptom of interest (SOI) against a large, heterogeneous lesion database (e.g., 1,100 lesions[11] spanning 26 symptoms such as aphasia, depression and central pain). Because such lesion pools aggregate largely unrelated conditions, the contrast approximates a near-random spatial distribution of lesions across the brain and achieves only "broad specificity", failing to resolve finer mixtures within a single symptom's map. For example, motor and visual anosognosia[12] likely engage both an anosognosia-general system (e.g., bodily self-awareness) and modality-specific motor or visual networks, yet conventional LNM yields a single entangled map that cannot disentangle the two[13]. This situation echoes early task neuroimaging[14,15], where task-versus-rest contrasts conflated multiple cognitive processes until the field shifted to task-versus-task comparisons with matched controls (e.g., memory encoding vs. retrieval[16]) to isolate specific functions. By analogy, LNM still lacks "selective specificity", a contrast against meaningfully related symptoms rather than heterogeneous reference pools. Consequently, how sensitivity analyses capture genuine functional networks beyond connectome-driven biases, and how to robustly distinguish symptom-specific patterns from related conditions, remain critical unresolved questions.

Here, we propose a "robust LNM" (rLNM) framework as a unified and statistically rigorous approach for sensitivity and specificity testing. First, to replace the arbitrary, whole-brain threshold with a region-specific null reference that accounts for connectome heterogeneity, we implement a spatial null model-based test for sensitivity testing (Fig. 1a, see Methods), similar in concept to that proposed by Zalesky and Cash[9]. If symptoms are genuinely underpinned by network disruptions, observed lesion-connectivity overlap should exceed what would arise from random lesion placements. Specifically, each lesion is randomly repositioned across the brain while preserving lesion size, shape, and inter-lesion overlap distribution via simulated annealing[17], yielding an anatomy-preserved null model of 10,000 synthetic LNM maps. The observed LNM map is then compared against this null distribution using voxel-wise testing to derive a null model-controlled sensitivity map. Second, to achieve selective specificity, rLNM enables hypothesis-driven contrasts between mechanistically or clinically related symptoms, isolating network effects unique to one condition beyond shared components. We formalize this contrast using a regression-based approach (Fig. 1b, see Methods): a cross-symptom map representing the shared component is derived from lesion-wise connectivity maps across the contrasted conditions, and then regressed out from each symptom's connectivity map to obtain symptom-specific residual maps. The statistical significance of these residuals is then assessed against a label-permutation null distribution, yielding the final selective specificity maps. Notably, beyond LNM itself, this framework is applicable to its derivatives, such as atrophy network mapping[18] and causal brain mapping[19].

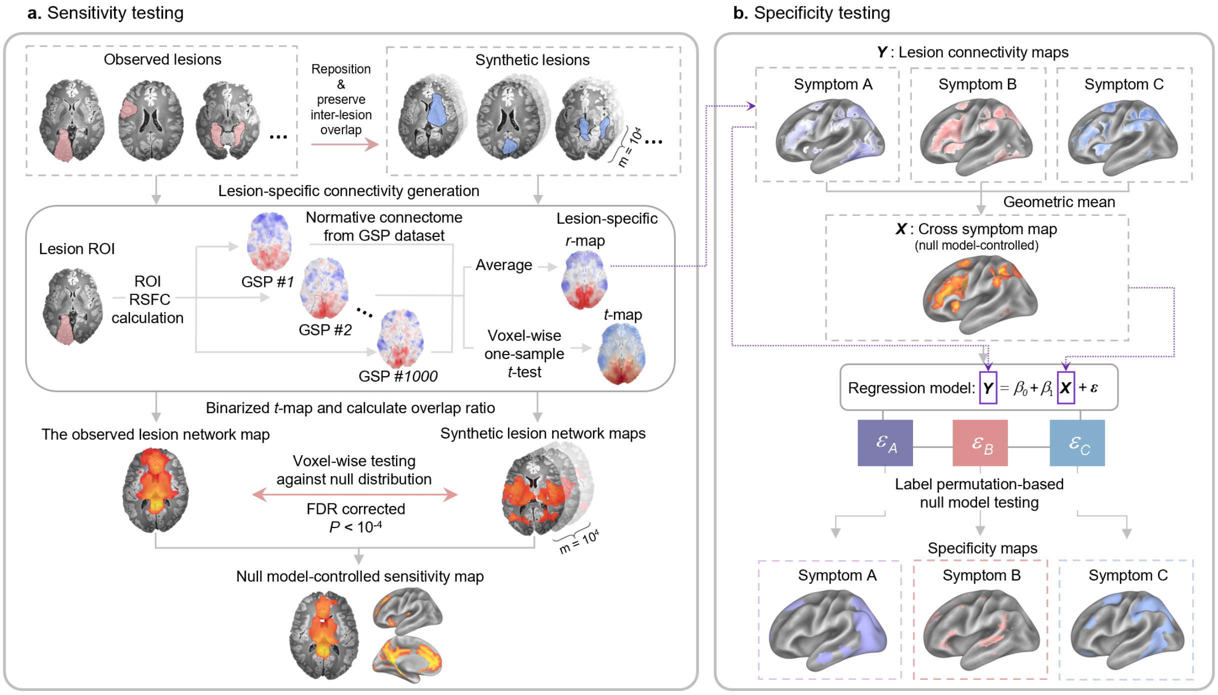

Fig. 1 | Overview of the robust lesion network mapping approach. a, Sensitivity testing. Observed lesion locations are first used to generate lesion-specific connectivity maps based on a normative connectome derived from 1000 healthy participants. The observed lesion network map is obtained by binarizing lesion-wise functional connectivity and calculating the overlap ratio. To assess statistical significance, a spatial null model-based testing framework is implemented, in which synthetic lesions are generated by randomly repositioning lesions across the brain while preserving lesion size, shape, and spatial overlap. For each repetition, synthetic lesion network maps are computed using the same pipeline as the observed lesions. Repeating this procedure 10,000 times yields a null distribution of lesion network maps. The observed map is then compared against this null distribution using voxel-wise testing ($P < 10^{-4}$, false discovery rate (FDR) corrected) to identify regions showing consistent connectivity across lesions. **b,** Specificity testing. Lesion connectivity maps (defined as the average functional connectivity across lesions) from contrasted symptoms are combined to derive a cross-symptom map capturing shared functional network. Using ordinary least squares regression, this shared component is regressed out from each connectivity map to obtain symptom-specific effects. Statistical significance is assessed using a label permutation-based null model, to identify network patterns that are specific to symptoms of interest.

To evaluate rLNM's performance, we first applied the rLNM framework to publicly available lesion datasets, including visual deficits[20] (*n* = 40), amnesia[21] (*n* = 43), stuttering[22] (*n* = 20), and migraine[23] (*n* = 11) for sensitivity testing (Fig. 2a & b). The null model-controlled sensitivity map of visual deficits predominantly localized to the visual cortex and lateral geniculate nucleus (LGN), as expected (Fig. 2a, left). The amnesia map highlighted the anterior/posterior cingulate cortex and hippocampus, which largely overlap with the DMN and are closely associated with memory function[24] (Fig. 2a, middle). In stuttering, significant effects were primarily observed in the putamen, which has been reported to exhibit morphological alterations in this disorder[25,26] (Fig. 2a right). In contrast, no region survived the null model-based test in migraine (Fig. 2b, left)., synthetic lesions (*n* = 100; Fig. 2b, middle) and mixed lesions (*n* = 100; randomly sampled from ten lesion datasets, see Methods; Fig. 2b, right), despite observed high overlap prior to null model-based testing. These results indicate that the rLNM reliably identifies symptom-related networks while robustly controlling for false-positive and false-negative findings.

To demonstrate how selective specificity decomposes mixed lesion maps, we examined motor (*n* = 95) and visual anosognosia (*n* = 24) [12], two conditions sharing an anosognosia-general symptom, while differing in sensory modality. Based on the sensitivity maps for each symptom type (Fig. 2c, left), we derived a cross-symptom map (Fig. 2c, middle), and highlighted a convergent region in the pars marginalis of the cingulate sulcus, overlapping with the previously defined subnetwork of the action mode network implicated in bodily self [27,28]. We next derived specificity maps for each condition (Fig. 2c, right), which predominantly involved the corresponding motor and visual systems, consistent with their distinct functional symptoms.

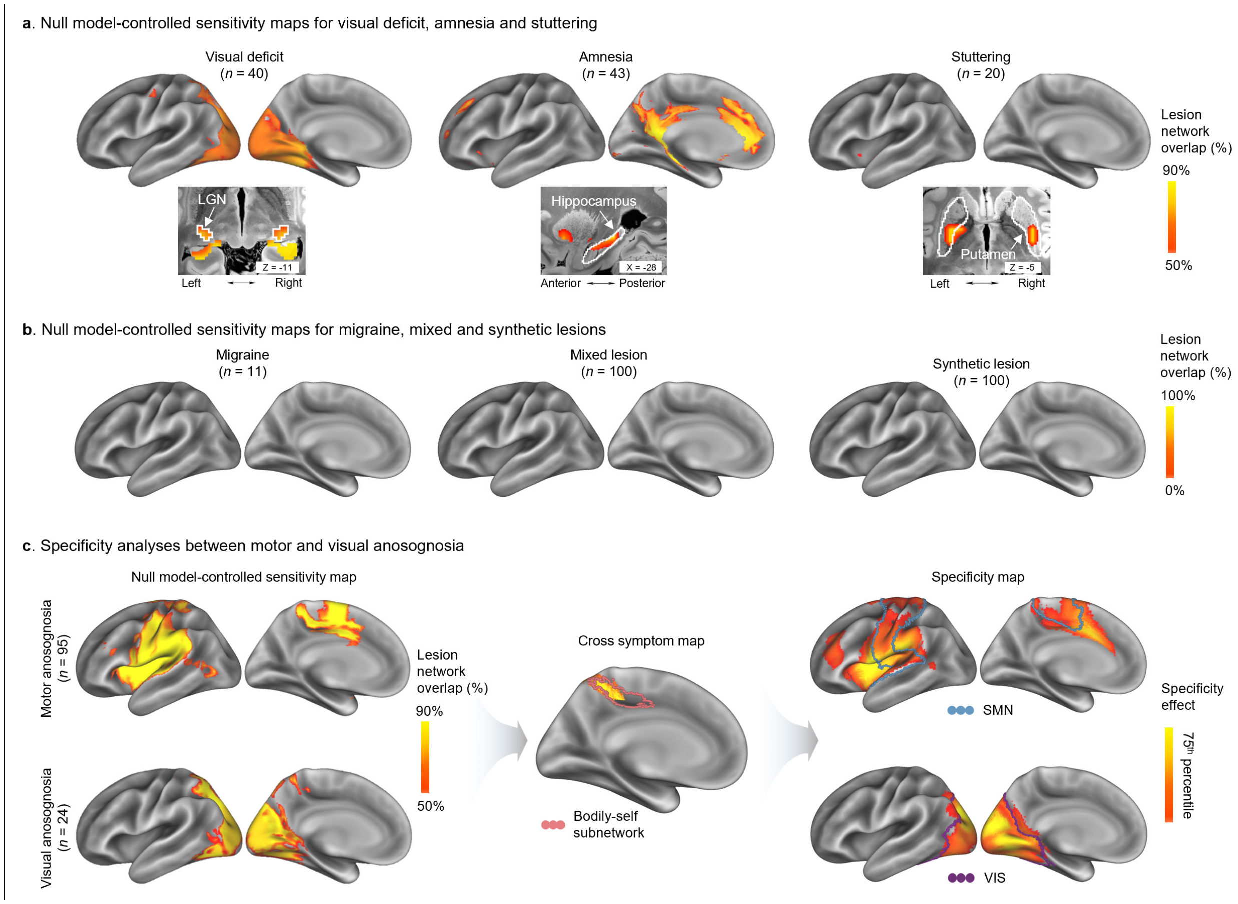

Fig. 2 | rLNM dissociates functional networks across and within neurological symptoms. a, Cortical and subcortical visualizations of null model-controlled sensitivity maps across three neurological conditions. The map for visual deficits (*n* = 40; left) highlights regions within the visual cortex and lateral geniculate nucleus (LGN). The map for amnesia (*n* = 43; middle) identifies the anterior/posterior cingulate cortex and hippocampus. The map for stuttering (*n* = 20; right) highlights the putamen. **b**, Cortical visualization of null model-controlled sensitivity maps derived from migraine (*n* = 11; left), mixed lesions (*n* = 100; middle), and synthetic lesions (*n* = 100; right). No regions survived null model-based testing in these conditions. **c**, Dissociation between cross-symptom and symptom-specific effects derived from motor (*n* = 95) and visual anosognosia (*n* = 24). In specificity analyses, based on the sensitivity maps for each condition (left), the cross-symptom map (middle) highly overlapped with the bodily-self subnetwork of the action mode network (pink boundary). The specificity maps for motor (upper right) and visual (lower right) anosognosia highlights the SMN (blue boundary) and visual (VIS, purple boundary) networks, respectively.

Because lesion-based analyses lack a ground-truth reference, we further benchmarked rLNM using activation network mapping (ANM)[2], a derivative of LNM in which task activation coordinates serve as seeds. Task activations from well-designed experiments converge on canonical functional networks, providing a priori reference against which rLNM's outputs can be judged. Task-based fMRI activation coordinates were sourced from the BrainMap database (see Methods). Null model-controlled sensitivity maps of social cognition (n = 248 experiments; Figure 3a, left), language (n = 155 experiments; Figure 3a, middle), and motor (n = 234 experiments; Figure 3a, right) tasks highlight the default mode network (DMN), language network (LAN), and somatomotor network (SMN), respectively. Comparative functional pattern analytics by the Neurosynth database[29] associates these maps with the terms "social" ($r = 0.43$, $P < 10^{-4}$, false discovery rate (FDR) corrected), "language" ($r = 0.57$, $P_{\mathrm{FDR}} < 10^{-4}$) and "motor" ($r = 0.59$, $P_{\mathrm{FDR}} < 10^{-4}$). For specificity analyses, we collected three types of working memory (WM) tasks: verbal (n = 38 experiments), face (n = 14 experiments) and visuospatial (n = 19 experiments) WM (Fig. 3b, left column). The cross-symptom map generated by aggregating these three tasks (Fig. 3b, top center) significantly correlated with the "working memory" map derived from the Neurosynth database ($r = 0.56$, $P_{\mathrm{FDR}} < 10^{-4}$; Fig. 3b, bottom center). We then derived specificity maps by regressing out the cross-symptom component, which remarkably reduced the high inter-map similarity observed prior to regression (pairwise r = 0.80, 0.71, and 0.76), resulting in maps with minimal spatial overlap ($r = 0$ for all pairs). These selective working memory specificity maps (right) highlighted regions of inferior frontal gyrus (IFG; verbal WM), fusiform face area (FFA; face WM), superior parietal lobule (SPL, visuospatial WM), respectively. The most associated NeuroSynth terms were "word" ($r = 0.33$, $P_{\mathrm{FDR}} < 10^{-4}$) for the verbal working memory selective specificity map, "face" ($r = 0.19$, $P_{\mathrm{FDR}} < 10^{-4}$) for the face working memory map, and "spatial" ($r = 0.13$, $P_{\mathrm{FDR}} < 10^{-4}$) for the visuospatial working memory map, indicating that the specificity testing effectively captured task-specific effects.

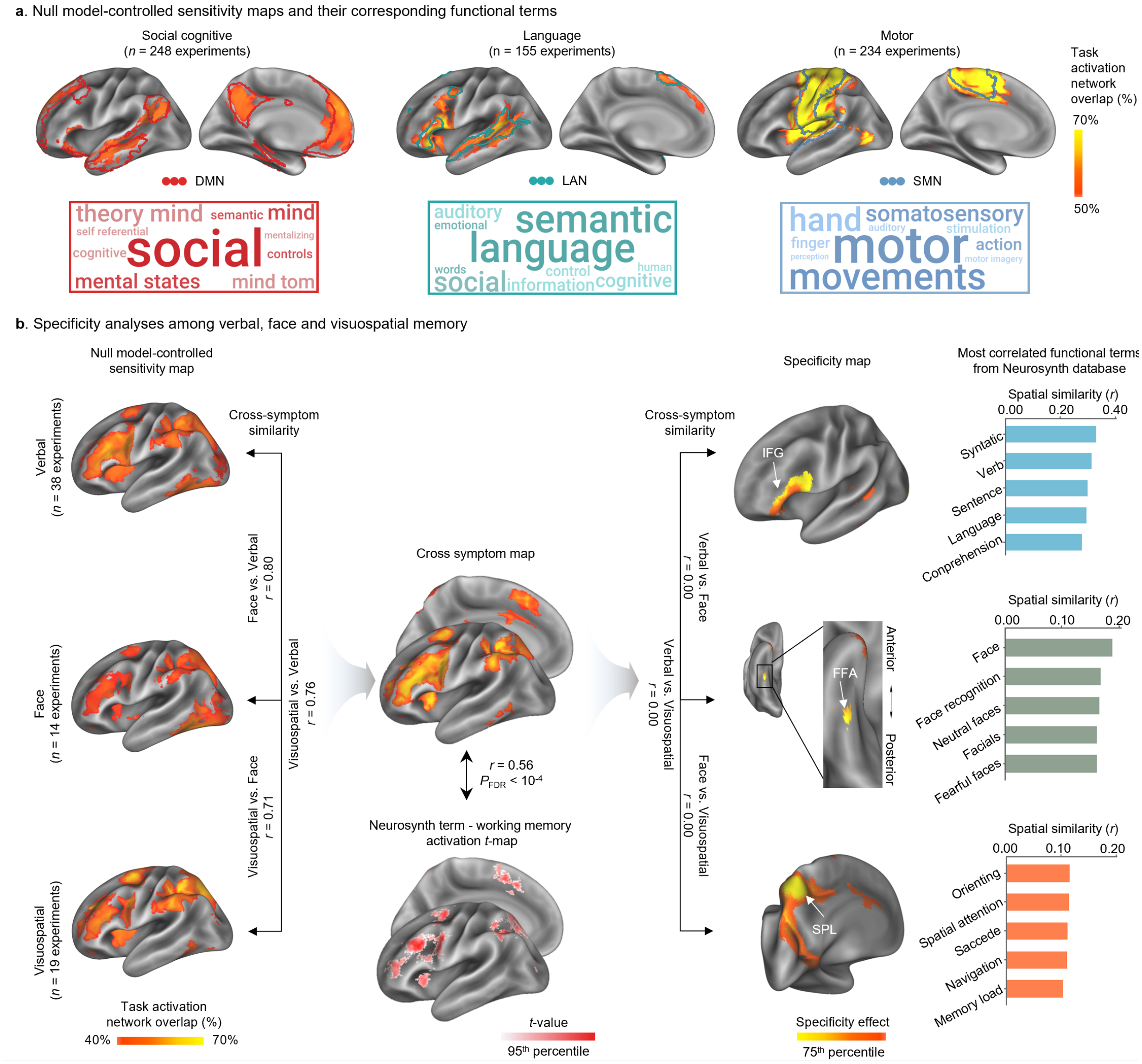

Fig. 3 | rLNM dissociates functional networks across and within cognitive domains. a, Null model-controlled sensitivity maps of three canonical cognitive domains and their corresponding functional terms. In sensitivity analyses, cortical surface visualization (top) of the rLNM-derived ANM maps for social cognition (n = 248 experiments), language (n = 155 experiments), and motor (n = 234 experiments) highlight key regions of the default mode network (DMN, red boundary), language network (LAN, green boundary) and somatomotor network (SMN, blue boundary), respectively. Word clouds (bottom) summarize their corresponding functional terms in the Neurosynth database, with font size scaled proportionally to correlation strength. **b**, Dissociation between cross-symptom and symptom-specific effects derived from working memory tasks. Based on the sensitivity maps (left) from verbal (n = 38 experiments), face (n = 14 experiments) and visuospatial (n = 19 experiments) work memory, the resulting cross-symptom map (middle) shows a significant spatial correspondence (Pearson's $r = 0.56$, $P_{\mathrm{FDR}} < 10^{-4}$) with the working memory activation map from the Neurosynth database. The specificity maps (right) reveal distinct patterns for each condition, highlighting regions of inferior frontal gyrus (IFG), fusiform face area (FFA), and superior parietal lobule (SPL), respectively. Bar plots display the most correlated terms from the Neurosynth database with each specificity map.

Recent debates[5-10] about the validity of LNM offer an important opportunity to revisit and improve its methodological foundations. Here, our rLNM reformulates the sensitivity testing by replacing arbitrary, whole-brain thresholds with an anatomy-preserving spatial null model. By comparing observed lesion connectivity overlap to region-specific null distributions, this approach provides explicit control over false-positive and false-negative rates, requiring stronger effects in hub regions (e.g., insula) while allowing more moderate overlap elsewhere to remain informative. In effect, this null model largely offers a self-contained alternative to “broad specificity” analyses, without requiring the need for large-scale external lesion datasets as a control.

In addition, rLNM reframes specificity testing from broad to selective contrasts (Fig. 1b), enabling direct comparisons between mechanistically or clinically related symptoms. Echoing the late-1990s shift in cognitive neuroimaging toward matched experimental contrasts[13,16], rLNM establishes a new paradigm for well-controlled, hypothesis-driven network-pattern inference. Together with rLNM’s sensitivity testing, this reframing may help explain why previously reported LNM maps across diverse conditions often exhibit substantial similarity[5]. Such similarity likely reflects both connectome-driven anatomical biases and an unresolved mixture of symptom-specific and symptom-general components, features that conventional LNM was not originally designed to disentangle. Our results further demonstrate that this framework generalizes from LNM to ANM, and is readily applicable to a broader class of pattern-based network inferences, such as imaging-transcriptomic mapping[30] and trans-diagnostic brain mapping[31]. As an open-source framework, rLNM thus provides a practical foundation for re-evaluating existing findings, while promoting transparency and standardization in future analyses.

Methods

Lesion Datasets

To assess the validity of the rLNM approach across a range of neuropsychiatric conditions, we assembled lesion datasets spanning 10 disorders from previously published studies and publicly available resources. These included visual deficits[20], amnesia[21], stuttering[22], migraine[23], visual and motor anosognosia[12], ataxia[33], alien limb syndrome[34], addiction[35], and neglect[20]. Lesion datasets for amnesia, stuttering, migraine, alien limb syndrome, addiction, and neglect were obtained from a previously curated resource[5]. The visual deficit dataset was obtained from an online lesion database (Lesion Bank; https://lesionbank.org). For anosognosia, motor anosognosia lesions were obtained from the publicly available data of the original study[12], whereas visual anosognosia lesions were manually delineated by a senior neuroradiologist based on lesion locations reported in the same study. The ataxia dataset was downloaded from the public data from the original study[33].

The visual deficit dataset included 40 patients with visual field defects, color agnosia, or both. The amnesia dataset included 43 patients with focal brain lesions associated with clinically evident episodic memory impairment; all cases presented with anterograde amnesia and were identified through a systematic Medline search of case reports describing acquired amnesia following focal brain lesions. The stuttering dataset included 20 participants with persistent developmental stuttering. The migraine dataset included neuroimaging coordinates of decreased gray matter volume derived from a voxel-based morphometry (VBM) meta-analysis (*n* = 11 regions). The anosognosia dataset included lesions associated with visual anosognosia (*n* = 24) and motor anosognosia (*n* = 95). The limb ataxia dataset comprised 35 patients with clinically confirmed newly-onset acute limb ataxia. The alien limb dataset included 48 patients with focal brain lesions associated with alien limb syndrome, identified from published case reports describing involuntary movements attributed to external control. The addiction dataset included 34 patients with focal brain lesions who were active daily smokers at the time of lesion onset. The neglect dataset included 34 patients.

To provide control conditions, we constructed mixed lesion datasets by combining lesions across the ten disorders. We also included a synthetic lesion dataset comprising 100 lesions derived from van den Heuvel et al[5]. Synthetic lesions were generated by randomly sampling atlas regions with uniform probability and then expanding each seed to include neighboring regions, and were subsequently mapped to corresponding voxels in standard MNI space for voxel-wise analyses.

Task Activation Coordinates

Following the PRISMA (Preferred Reporting Items for Systematic Reviews and Meta-Analyses) guidelines (http://www.prisma-statement.org), we systematically identified functional neuroimaging studies from the BrainMap database (www.brainmap.org), a large-scale repository encompassing over 130,000 experiments. In this study, we focused on four core cognitive tasks[32]: social cognition (theory of mind), language, motor, and working memory.

To ensure data quality and homogeneity, we applied the following inclusion criteria across all domains: (1) use of fMRI or PET imaging; (2) involvement of healthy adult participants only (experimental context: normal mapping); (3) reporting of whole-brain results in standard stereotactic space (MNI or Talairach); and (4) inclusion of activation data only (experimental activation: activations only). Beyond these universal standards, we developed task-specific search strategies to capture the unique functional architecture. For language, we combined the “cognition–language” with a specific “language” context. For social cognition, we focused on the "theory of mind" paradigm to isolate core mentalizing processes. For motor function, we restricted analyses to simple "flexion/extension" tasks to minimize contributions from higher-order motor planning. For working memory, we selected the well-established "n-back" paradigm to ensure consistency across studies. The final meta-analytic dataset comprised: social cognition (62 papers, 248 experiments, 1,187 participants, 1,736 foci); language (33 papers, 155 experiments, 964 participants, 1,075 foci); motor (74 papers, 234 experiments, 2,173 participants, 3,892 foci); and working memory (137 papers, 426 experiments, 4,267 participants, 3,448 foci).

To investigate the symptom-specific effects, we performed a sub-stratification of the working memory dataset. Based on detailed inspection of experimental metadata, studies were categorized according to their stimulus modality, and the following categories were included: verbal (e.g., words or sentences; 38 experiments), face (e.g., human faces; 14 experiments), and visuospatial (e.g., spatial locations or navigation; 19 experiments) working memory.

MRI data and preprocessing

Resting-state fMRI data from 1,000 healthy participants in the Brain Genomics Superstruct Project (GSP)[36] were used to construct a normative connectome. Preprocessing of both structural and functional MRI data was performed using DeepPrep[37-39] with parameters consistent with our previous studies[40,41]. The fMRI preprocessing pipeline included the following steps: (1) slice timing correction; (2) head motion correction; (3) linear detrending and bandpass filtering within the range of 0.01-0.08 Hz; and (4) regression to account for nuisance variables, which encompassed the six motion parameters, white matter signal, ventricular signal, global signal and their first-order temporal derivatives. Volumetric fMRI data were normalized to a 2-mm isotropic template (the FSL version of the MNI ICBM152 nonlinear template), followed by spatial smoothing using a 6-mm full-width at half-maximum (FWHM) isotropic Gaussian kernel within the brain mask. For rLNM, all lesion masks were first normalized to the same 2-mm isotropic volumetric template using a 12-degree-of-freedom linear transformation (FSL v6.0)[42]. In this study, rLNM analyses were conducted in a downsampled 8-mm isotropic space to reduce computational complexity. For visualization, volumetric data were resampled to 1-mm resolution, and projected onto the surface-based fsaverage standard space using FreeSurfer[43]. In future applications, we recommend performing rLNM analyses in 2-mm isotropic space to achieve finer spatial resolution.

Sensitivity validation

To evaluate the sensitivity of symptom-related functional networks and control for false-positive and false-negative findings, we incorporated a null model-based testing into conventional LNM framework. We first constructed an observed LNM map using true lesions. Each lesion was treated as an individual region of interest (ROI), and its resting-state functional connectivity (RSFC) profile was estimated using normative rs-fMRI data from 1,000 healthy participants in the GSP dataset[36]. For each healthy participant, the mean BOLD time series within each ROI was extracted and correlated with the time series of all other brain voxels. Correlation coefficients were normalized using Fisher's r-to-z transformation, yielding individual RSFC maps. For each ROI, voxel-wise one-sample t-tests were performed across the 1,000 RSFC maps and followed by false discovery rate (FDR) correction ($P < 0.01$) to obtain ROI-specific t-maps. These maps were thresholded at $|t| > 7$ and binarized (see Supplementary Note for details), then aggregated by computing voxel-wise overlap proportions across all lesions, yielding an observed LNM map.

To assess statistical significance of the observed LNM map, we implemented a spatial null model–based testing that constrains lesion size, shape, and spatial overlap[9]. Specifically, synthetic lesions were randomly repositioned across the brains under these constraints. A global optimization procedure based on simulated annealing[17] was used to match the inter-lesion overlap distribution between synthetic and observed lesions, with similarity (quantified via two-sample *t*-test) as the objective function. For each iteration, ROI-specific *t*-maps were then computed for the synthetic lesions using the same pipeline as the observed lesions. This process was repeated 10,000 times to generate a null distribution of LNM maps. The observed LNM map was subsequently compared against this distribution using voxel-wise testing to derive a statistical *P*-map, defined as the proportion of synthetic map values exceeding the observed map at each voxel. After FDR correction, voxels with $P_{\mathrm{FDR}} < 10^{-4}$ were retained to define the final null model-controlled sensitivity map.

Specificity validation

Specificity validation aims to identify functional patterns that distinguish a symptom from related but distinct conditions. This procedure comprises three steps. First, a cross-symptom map was constructed to capture shared functional patterns across symptoms. Specifically, for each symptom, connectivity maps were obtained by averaging ROI-specific connectivity profiles (defined as mean functional connectivity across 1,000 healthy subjects from the GSP dataset) across lesions. Only voxels showing positive functional connectivity across all symptoms were retained. The cross-symptom map was then computed as the voxel-wise geometric mean of these maps, isolating a core network consistently expressed across symptoms. To restrict this network to statistically robust regions, the resulting map was further masked by voxels surviving sensitivity validation (i.e., null model-based permutation testing with 10,000 iterations), yielding the final cross-symptom connectivity map.

Second, symptom-specific effects were derived using a regression framework. The cross-symptom map was used as the sole predictor in an ordinary least squares model, and the shared component was regressed out from each symptom connectivity map, respectively. The resulting residuals were standardized using whole-brain Z-scoring, yielding maps of symptom-specific effects.

Third, statistical significance of the symptom-specific effects was assessed using a label permutation-based null model. Specifically, lesion labels were randomly reassigned across symptoms while preserving sample size, and synthetic symptom connectivity maps were recomputed. The same regression procedure was applied to obtain null residual maps. This process was repeated 10,000 times to generate a null distribution of symptom-specific effects. Voxel-wise P values were computed as the proportion of null effects exceeding the observed effects. After FDR correction, voxels with $P_{\mathrm{FDR}} < 10^{-4}$ were retained to define the final specificity maps.

Comparative functional pattern analytics

To characterize the cognitive and behavioral correlates of LNM maps, we performed a spatial meta-analytic comparison using the NeuroSynth database (https://neurosynth.org/)[29]. Neurosynth provides whole-brain activation maps for 1,334 functional patterns, which are derived from large-scale meta-analyses of neuroimaging studies. These maps represent how fluctuations in regional brain activity correspond to specific psychological processes. In our analysis, anatomical terms (e.g., “insula” and “cortical”) and repetitive patterns were excluded, restricting the analysis to cognitive and behavioral domains. Spatial similarity between LNM maps and each functional map was quantified using voxel-wise Pearson correlation coefficients.

Data availability

The normative rs-fMRI data from GSP used for functional connectivity analyses are publicly available at https://dataverse.harvard.edu/dataverse/GSP. The cortical parcellation atlas is publicly available at https://surfer.nmr.mgh.harvard.edu/fswiki/CorticalParcellation_Yeo2011. The volumetric brain template is an ultrahigh-resolution ex-vivo brain in MNI space[44], which is available at https://datadryad.org/stash/downloads/file_stream/182489.

Code availability

The codes for the proposed framework will be available. Software packages incorporated into the above code for data analysis included: Matlab R2020a, https://www.mathworks.com/; Python v3.11.6, https://www.python.org; MRIcroN v1.0; Connectome Workbench v1.5, http://www.humanconnectome.org/software/connectome-workbench.html; Freesurfer v6.0.0, https://surfer.nmr. mgh.harvard.edu/; FSL v6.0, https://fsl.fmrib.ox.ac.uk/fsl/fslwiki.

Acknowledgment

This work was supported by the Changping Laboratory (H.L., J.R.); National Institutes of Health grants MH096773 (N.U.F.D.), MH122066 (E.M.G., N.U.F.D.), MH121276 (E.M.G., N.U.F.D.), MH124567 (E.M.G., N.U.F.D.), NS129521 (E.M.G., N.U.F.D.), and NS088590 (N.U.F.D.); the Intellectual and Developmental Disabilities Research Center (N.U.F.D.); by the Kiwanis Foundation (N.U.F.D.); and the Washington University Hope Center for Neurological Disorders (E.M.G., N.U.F.D.).

Author contributions

Conception: H.L., J.R. and W.C. Design: W.C., J.Z., Y.L. and J.R. Data acquisition, analysis and interpretation: W.C., J.Z, Y.L., Y.Y., W.Z., J.H., F.W., E.M.G., J.R. and H.L. Manuscript writing and revision: W.C., J.Z., Y.L., E.M.G., N.U.F.D., D.W., J.R., and H.L. All authors approved the final manuscript.

Competing interests

H.L. serves as Chief Scientist and co-founder of Neural Galaxy Inc. and Galaxy Brain Scientific LLC. W.C., J.H., and D.W., J.R. serve on the scientific consulting board of Galaxy Brain Scientific LLC. These relationships were reviewed and managed in accordance with institutional conflict-of-interest policies at Changping Laboratory. N.U.F.D. has a financial interest in Turing Medical Inc. and may financially benefit if the company is successful in marketing FIRMM motion monitoring software products. E.M.G. and N.U.F.D. may receive royalty income based on FIRMM technology developed at Washington University School of Medicine and licensed to Turing Medical Inc. N.U.F.D. is a co-founder of Turing Medical Inc. These potential conflicts of interest have been reviewed and are managed by Washington University School of Medicine. Other authors declare no conflict of interest regarding the publication of this work.

References

1 Fox, M. D. Mapping symptoms to brain networks with the human connectome. *New England Journal of Medicine* **379**, 2237-2245 (2018).

2 Peng, S., Xu, P., Jiang, Y. & Gong, G. Activation network mapping for integration of heterogeneous fMRI findings. *Nature human behaviour* **6**, 1417-1429 (2022).

3 Makhlouf, A. T. *et al.* Heterogeneous patterns of brain atrophy in schizophrenia localize to a common brain network. *Nature Mental Health* **3**, 19-30 (2025).

4 Siddiqi, S. H. *et al.* Brain stimulation and brain lesions converge on common causal circuits in neuropsychiatric disease. *Nature human behaviour* **5**, 1707-1716 (2021).

5 van den Heuvel, M. P. *et al.* Investigating the methodological foundation of lesion network mapping. *Nature Neuroscience*, 1-11 (2026).

6 Siddiqi, S. *et al.* The methodological foundations of lesion network mapping remain sound. *bioRxiv*, 2026.2002. 2024.707529 (2026).

7 Meng, Y. *et al.* The diversity of lesion network mapping findings. *bioRxiv*, 2026.2002. 2012.705312 (2026).

8 Petersen, M., Patil, K. R., Eickhoff, S. B. & Biessels, G. J. Permutation-based inference preserves anatomical specificity in lesion network mapping. *medRxiv*, 2026.2002. 2016.26346377 (2026).

9 Zalesky, A. & Cash, R. F. Null models for lesion network mapping. *Nature Neuroscience*, 1-4 (2026).

10 Edelman, S., Elias, U. & Arzy, S. Dimensionality reduction establishes specificity in lesion network mapping. *medRxiv*, 2026.2001. 2029.26345138 (2026).

11 Al-Fatly, B. *et al.* Lesion network of oculogyric crises maps to brain dopaminergic transcriptomic signature. *Brain* **147**, 1975-1981 (2024).

12 Kletenik, I., Gaudet, K., Prasad, S., Cohen, A. L. & Fox, M. D. Network localization of awareness in visual and motor anosognosia. *Annals of neurology* **94**, 434-441 (2023).

13 Poldrack, R. A. Can cognitive processes be inferred from neuroimaging data? *Trends in cognitive sciences* **10**, 59-63 (2006).

14 Demonet, J., Wise, R. & Frackowiak, R. Language functions explored in normal subjects by positron emission tomography: A critical review. *Human Brain Mapping* **1**, 39-47 (1993).

15 Petersen, S. E., Fox, P. T., Posner, M. I., Mintun, M. & Raichle, M. E. Positron emission tomographic studies of the processing of singe words. *Journal of cognitive neuroscience* **1**, 153-170 (1989).

16 Wagner, A. D. *et al.* Building memories: remembering and forgetting of verbal experiences as predicted by brain activity. *Science* **281**, 1188-1191 (1998).

17 Kirkpatrick, S., Gelatt Jr, C. D. & Vecchi, M. P. Optimization by simulated annealing. *science* **220**, 671-680 (1983).

18 Tetreault, A. M. *et al.* Network localization of clinical, cognitive, and neuropsychiatric symptoms in Alzheimer's disease. *Brain* **143**, 1249-1260 (2020).

19 Siddiqi, S. H., Kording, K. P., Parvizi, J. & Fox, M. D. Causal mapping of human brain function. *Nature reviews neuroscience* **23**, 361-375 (2022).

20 Turner, J. *et al.* in *Neurology.* 6856 (Lippincott Williams & Wilkins Hagerstown, MD).

21 Ferguson, M. A. *et al.* A human memory circuit derived from brain lesions causing amnesia. *Nature communications* **10**, 3497 (2019).

22 Theys, C. *et al.* Localization of stuttering based on causal brain lesions. *Brain* **147**, 2203-2213 (2024).

23 Burke, M. J. *et al.* Mapping migraine to a common brain network. *Brain* **143**, 541-553 (2020).

24 Menon, V. 20 years of the default mode network: A review and synthesis. *Neuron* **111**, 2469-2487 (2023).

25 Chow, H. M., Garnett, E. O., Koenraads, S. P. & Chang, S.-E. Brain developmental trajectories associated with childhood stuttering persistence and recovery. *Developmental cognitive neuroscience* **60**, 101224 (2023).

26 Neef, N. E. *et al.* Altered morphology of the nucleus accumbens in persistent developmental stuttering. *Journal of Fluency Disorders* **55**, 84-93 (2018).

27 Badke D'Andrea, C. *et al.* Action-mode subnetworks for decision-making, action control, and feedback. *Proceedings of the National Academy of Sciences* **122**, e2502021122 (2025).

28 Lyu, D. *et al.* Causal evidence for the processing of bodily self in the anterior precuneus. *Neuron* **111**, 2502-2512. e2504 (2023).

29 Yarkoni, T., Poldrack, R. A., Nichols, T. E., Van Essen, D. C. & Wager, T. D. Large-scale automated synthesis of human functional neuroimaging data. *Nature methods* **8**, 665-670 (2011).

30 Fornito, A., Arnatkevičiūtė, A. & Fulcher, B. D. Bridging the gap between connectome and transcriptome. *Trends in cognitive sciences* **23**, 34-50 (2019).

31 Goodkind, M. *et al.* Identification of a common neurobiological substrate for mental illness. *JAMA psychiatry* **72**, 305-315 (2015).

32 Dm, B. *et al.* Function in the human connectome: task-fMRI and individual differences in behavior. *Neuroimage* **80**, 169-189 (2013).

33 Liesmäki, O. *et al.* Localization and network connectivity of lesions causing limb ataxia in patients with stroke. *Neurology* **103**, e209803 (2024).

34 Darby, R. R., Joutsa, J., Burke, M. J. & Fox, M. D. Lesion network localization of free will. *Proceedings of the National Academy of Sciences* **115**, 10792-10797 (2018).

35 Joutsa, J. *et al.* Brain lesions disrupting addiction map to a common human brain circuit. *Nature medicine* **28**, 1249-1255 (2022).

36 Holmes, A. J. *et al.* Brain Genomics Superstruct Project initial data release with structural, functional, and behavioral measures. *Scientific data* **2**, 1-16 (2015).

37 Ren, J. *et al.* DeepPrep: an accelerated, scalable and robust pipeline for neuroimaging preprocessing empowered by deep learning. *Nature Methods*, 1-4 (2025).

38 Ren, J. *et al.* Fast cortical surface reconstruction from MRI using deep learning. *Brain informatics* **9**, 6 (2022).

39 Ren, J. *et al.* SUGAR: Spherical ultrafast graph attention framework for cortical surface registration. *Medical Image Analysis* **94**, 103122 (2024).

40 Wang, F. *et al.* Verbal memory network mapping in individual patients predicts postoperative functional impairments. *Human Brain Mapping* **45**, e26691 (2024).

41 Dahmani, L. *et al.* Focused ultrasound thalamotomy for tremor treatment impacts the cerebello-thalamo-cortical network. *npj Parkinson's Disease* **9**, 90 (2023).

42 Smith, S. M. *et al.* Advances in functional and structural MR image analysis and implementation as FSL. *Neuroimage* **23**, S208-S219 (2004).

43 Fischl, B. FreeSurfer. *Neuroimage* **62**, 774-781 (2012).

44 Edlow, B. L. *et al.* 7 Tesla MRI of the ex vivo human brain at 100 micron resolution. *Scientific data* **6**, 244 (2019).